Journal Pre-proof

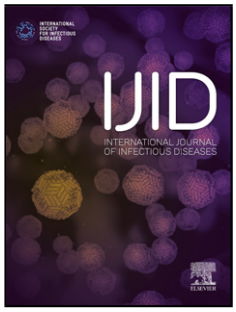

Paromomycin: a potential dual targeted drug effectively inhibits both Spike (S1) and Main Protease of COVID-19

Asma Tariq, Rana Muhammad Mateen, Muhammad Sohail Afzal, Mahjabeen Saleem

PII: S1201-9712(20)30498-7

DOI: https://doi.org/10.1016/j.ijid.2020.06.063

Reference: IJID 4368

To appear in: *International Journal of Infectious Diseases*

Please cite this article as: { doi: https://doi.org/

Title: Paromomycin: a potential dual targeted drug effectively inhibits both Spike (S1) and Main Protease of COVID-19

Asma Tariq[a], Rana Muhammad Mateen[b], Muhammad Sohail Afzal[b], Mahjabeen Saleem[a]

[a] Institute of Biochemistry and Biotechnology, University of the Punjab, Lahore, Pakistan.

[b] Department of Life sciences, School of Science, University of Management and Technology, Lahore, Pakistan.

Correspondence to: Asma Tariq, Institute of Biochemistry and Biotechnology, University of the Punjab, Lahore, Pakistan. (e-mail: asmi_mahmood@yahoo.com), Phone No.: 0923314325583.

Author's Emails:

Asma Tariq: asmi_mahmood@yahoo.com, Rana Muhammad Mateen: mateenibb@yahoo.com, Muhammad Sohail Afzal: sohail.ncvi@gmail.com, Mahjabeen Saleem: mahjabeen.ibb@pu.edu.pk

Highlights

- With increase in number of people suffering from COVID-19, there is a dire need to look for effective remedies against this pandemic.
- In this study, we propose a single drug Paromomycin against two targets of COVID-19 i.e. Spike protein (S1) and protease domain. Based upon docking scores and MD simulation, Paromomycin was found to have strong binding affinity against both the targets of coronavirus.
- 15 anti-malarial drugs including chloroquine were also investigated against both targets using in-silico approach. The results showed that no anti-malarial drug exhibited effective binding against either S1 or protease.

- Paromomycin, a broad spectrum aminoglycoside antibiotic that is originally used to treat acute and chronic intestinal infection may also be potentially used to treat COVID-19. As one of the major symptoms in COVID-19 infection include GI disturbance.
- Clinical trials are further needed to confirm the efficacy of Paromomycin against COVID-19.

Abstract

Objectives: With increase in number of people suffering from COVID-19, there is a dire need to look for effective remedies against this pandemic. Drug repurposing seems to be the solution for current situation.

Methods: In our quest for finding potential drug against this virus, 15 anti-malarial drugs including chloroquine, and 2413 FDA approved drugs were investigated against both protease and spike proteins of COVID-19 using *in-silico* approach. Molecular docking analysis followed by MD simulation was carried out to estimate the binding and stability of the complexes.

Results: In this study, we found a single drug Paromomycin against two targets of COVID-19 i.e. Spike protein (S1) and protease domain. Paromomycin was found to have strong binding affinity against both the targets of coronavirus. The results also showed that no anti-malarial drug exhibited effective binding against either S1 or protease.

Conclusions: Current study concluded that Paromomycin is an effective dual targeting drug against coronavirus, as it binds not only to the protease domain of the virion but also with the

spike domain with high stability. Furthermore, none of the anti-malarial drugs showed strong binding affinity for either protease or receptor binding domain (RBD).

Keywords: COVID-19, drug repurposing, chloroquine, protease, spike, MD simulation

1. Introduction

Originating in December 2019 in Wuhan district of China, coronavirus (COVID-19) outbreak has spread all over the world creating a menace in the world community. Birds and wild animals have been suggested to be the spread of this novel virus (Wu et al. 2020; Zhou et al. 2020). According to the current statistics of WHO, total 1,696,588 confirmed cases of corona and 105, 952 associated deaths have been globally reported (WHO 2020). Currently no vaccine or effective drug is available for treatment of this disease and clinicians are treating with neutralizing antibodies used against SARS-CoV and MERS-CoV for targeting spike proteins of this virus (Chen et al. 2020a; Duan et al. 2020). As suggested in the recent research, spike protein which is present on the surface of novel coronavirus, interacts with the host's target such as, CD26 and ACE2; so is considered a potential and logical therapeutic target (Hoffmann et al. 2020; Zhang et al. 2020a).

Recent studies have shown the effectiveness of chloroquine against COVID-19, both in vitro and in clinical trials in China. In addition some modifications of chloroquine such as, sulfate and phosphate salts of chloroquine have also proved beneficial (Gao et al. 2020; Hu et al. 2020; Wang et al. 2020). However, FDA has not yet approved this drug for the treatment of COVID-19 and there is a dire need for further clinical trials conducted on geographically different populations to ascertain the effect of this drug.

Human Coronaviruses are single stranded positive sense RNA viruses which comprise of two groups of proteins: structural proteins, including S (Spike) proteins, M (Matrix) protein, N (Nucleocapsid) proteins and E (Envelope) proteins, and non- structural proteins include proteases such as, nsP3, nSP5 and RdRp such as nsp12. Spike protein is present in homo-trimeric form in the outer surface of the virion particle. There are two or three proteases encoded by the viral RNA, which are potential drug targets against the coronavirusus (Chen et al. 2020b; Vankadari and Wilce 2020). It has been established that this protein plays a vital role for attachment of viral entry in the host cell. Moreover, coronavirus spike protein enter into the host cell through angiotensin-converting-enzyme 2 (ACE2) receptors present on the lung epithelial cells and intestinal cells, causing lung disease and diarrhea. S1 and S2 RBD of the spike proteins attach to the ACE2, thus viral envelope attaches to the membrane and gets internalized (Ge et al. 2013; Wan et al. 2020). Another potential target in treating COVID-19, is the main protease enzyme considered a central enzyme in regulating viral replication and transcription (Jin et al. 2020).

There were two main objectives of this study: to determine the efficiency of the anti- malarial drugs against COVID-19 using *in-silico* approach and to purpose a single potential drug which acts against COVID-19 spike protein (S1) and also against catalytic domain of its protease protein.

2. Methods

2.1. Structures retrieval and pre-processing

The X-ray crystal structure of unliganded protease and RBD of S1 of the novel COVID-19 were retrieved from PDB repository as IDs: 6y84 (Resolution: 1·39 Å) and 6vw1 (Resolution: 2·68 Å) respectively. Both the structures were checked for errors and quality using Saves server.

Discovery studio visualizer (Dassault Systèmes BIOVIA, Discovery studio visualizer, v19·10·18287, San Diego: Dassault Systèmes, 2019) was used to examine the structural aspects of both the proteins specifically of 6vw1 for the receptor binding residues. After defining ligand (A chain: Angiotensin-converting enzyme 2; ACE2) and receptor (E chain: RBD), the interacting residues of A chain and E chain of 6VW1 were listed for further use in grid generation and docking analysis.

2.2. Molecular Docking analysis

2.2.1. Selection and Preparation of Ligands:

3D structures of 15 antimalarial drugs (Table 1) were retrieved from NCBI PubChem Compound database (https://pubchem.ncbi.nlm.nih.gov/), while 3D structures of 2413 FDA approved drugs were obtained from Drugbank (https://www.drugbank.ca/).

All ligand compound were prepared by Ligprep of the Maestro 12·2 (Schrödinger Release 2019-4: LigPrep, Schrödinger, LLC, New York, NY, 2020 using OPLS_2005 force field in Epik mode applying parameter such as generate possible states at target pH (pH: 7), desalting of ligands and tautomers generation while retaining specific chiralities to generate at most one per ligand. General study strategy for these ligands' analysis is summarized in Figure 1.

2.2.2. Proteins preparation and Glide docking:

Protein is prepared using the Schrodinger 12·2 protein preparation wizard (*Schrödinger Release 2019-4: Protein Preparation Wizard; Epik, Schrödinger, Prime, Schrödinger, LLC, New York, NY, 2020*) as described elsewhere (Sastry et al. 2013). Briefly, protein parameters were applied as addition of hydrogen atoms, assigning bond orders, creation of zero-order bonds to

metal, creation of disulphide bonds, deleting waters beyond 5Å, generation het states using Epik at pH: 7. After pre-processing any already attached ligands were removed and protein structures were corrected if needed by adding side-chain and missing atoms etc., followed by minimization and optimization using OPLS_2005 force field. All the active site residues of both proteins including catalytic diad and associated residues of 6y84 and RBD residues of 6vw1 were used in receptor grid generation. In receptor grid, x,y,z coordinates were supplied according to the grid size around the mentioned residues and grids were generated using default options. GLIDE molecular docking was carried out under default conditions in extra-precision mode (XP) (Schrödinger Release 2019-4: Glide, Schrödinger, LLC, New York, NY, 2020). Glide uses a series of scoring functions in XP mode to identify the optimal binding site of ligand for acceptable poses (Friesner et al. 2006). Top ranked ligands were selected on the basis of glide score (G score in Kcal / mol) in order to define the strength of protein-ligand interaction. Protein residue interactions of docked complexes were visualized and examined in Discovery studio visualizer (Dassault Systèmes BIOVIA, Discovery studio visualizer, v19·10·18287, San Diego: Dassault Systèmes, 2019).

2.3. Molecular dynamics simulation

The Molecular dynamics (MD) simulations of the top-ranked docked complexes were performed using Nano Scale Molecular Dynamics (NAMD); it works with CHARMM++ force field potential functions and parameters (Phillips et al. 2005),(Brooks et al. 2009),(Lee et al. 2016). The topologies and parameter files of proteins and ligand were generated in CHARMM-GUI using PDB Reader and Ligand Reader & Modeler respectively (Jo et al. 2008),(Jo et al. 2014),(Kim et al. 2017). The CHARMM36 force field is applied to protein at constant number of molecule, volume and temperature (NVT), and solvated the system by using Add solvation Box

with TIP3p water. Before simulation, each system was first energy-minimized and equilibrated for 200 ps followed by observing the total energy in multiplot. The energy-minimized systems were subsequently utilized to conduct simulations at constant temperature conditions (310 K) using Langevin dynamics parameters and under constant Periodic Boundary conditions for 50 ns for comparative trajectory analysis. The Visual Molecular Dynamics (VMD 1.9.3) was used to analyze the trajectories and for the post simulation analysis (Humphrey, William, Andrew Dalke 1996).

2.3.1. Post simulation analysis of trajectories

The dynamic properties of the complexes in comparison to individual proteins were studied to investigate the stability of the interacting residues. For this purpose, binding energy, root-mean-square deviation (RMSD), root mean square fluctuation (RMSF) and per-residue hydrogen bonding interactions were calculated using VMD. The free binding energy was estimated using Molecular Mechanics Poisson-Boltzmann Surface Area method (MMPBSA) in CaFE1.0 VMD plugin. The net energy of the system was estimated through the following equation (Liu and Hou 2016),

$$\Delta G_{binding} = G_{complex} - (G_{protein} + G_{ligand})$$

$$\Delta G_{bind} = \Delta H - T\Delta S = \{\Delta E_{gas} + \Delta G_{polarsol} + \Delta G_{nonpolarsol} - T\Delta S\}$$

For post simulation analysis, last 10ns trajectory was selected by extracting 1000 continues frames without stride. For MMPBSA, data was collected for every 5 ps and calculated for MM (NAMD), PB (APBS) and SA (VMD) values. In APBS calculations, interior dielectric constant was set to 2.0 with exterior dielectric constant as 80 (Wang and Kollman 2000; Li et al. 2018).

3. Results

3.1. Structural aspects of 6vw1 and 6y84

The crystal structure of 6vw1 consists of four chains: A, B, E, F among them A and B belong to human ACE2 receptor, are identical chains consisting of 571 residues each while E and F are identical chains comprising of 217 residues each belong to virion. The E chain residues interacting with ACE2 (A chain) include Arg-439, Tyr-449, Tyr-453, Leu-455, Phe-456. Ala-475, Glu-484, Phe 486, Asn-487, Tyr-489, Gln-493, Gly-496, Gln-498, Thr-500, Gly-502 and Tyr-505. In addition, ACE2 (A chain) residues interacting with COVID-19 RBD (chain A) include Ser-19, Gln-24, Lys-31, His-34, Glu-35, Glu-37, Asp-38, Tyr-41, Gln-42, Met-82, Tyr-83, Glu-329, Lys-353, Gly-354 (Figure 2). Structure of 6y84 comprises of a single chain A of 306 residues among those two residues are considered of making catalytic dyad i.e.; His-41 and Cys-145. Furthermore, some other residues at positions 442, 472, 479, 487,and 491 in spike protein of SARS-CoV protein were reported to play an important role in inter and intra species transmission of virus (Xintian et al. 2020).

3.2. Molecular Docking analysis of anti-malarial drug

Fifteen different anti-malarial drugs available in the market were docked against 6vw1 and 6y84 adopting two different strategies. In the first strategy, all antimalarial drugs were docked against specific residues (mentioned above) in both proteins while in second strategy whole protein grid was used to dock each drug for performing blind docking. Glide scores were calculated and were analyzed to check the binding efficiency of these drugs (Table 1).

3.3. Molecular Docking analysis of FDA approved drugs

2413 FDA approved drugs were used to study the effective binding against catalytic site of protease (6y84) and RBD of spike protein (6vw1) (Table S5-S10). For the entire data set of drugs, a distribution plot of docking scores was made (Figure 3). Top ranked drugs were selected on the basis of glide score (Table 2). Top three drugs against protease domain include Acarbose, Colistin and Paromomycin with glide scores -13·139, -12·63 and -11.5·79 respectively. On the other hand, Framycitin, Acarbose and Paromomycin drugs showed the high binding affinity for the RBD with glide scores -11·233, -10·49 and -10·01 respectively.

3.4. Tatuomeric forms of Paronomycin and their docking analysis

There are 11 tatuomeric forms of paronomycin (I-XI) due to alternate protonation state of its amide groups (Figure 1S). To elucidate further, both the proteins (6y84 and 6vw1) were docked against these 11 tatuomeric forms (Table S11, S12). It has been observed that both proteins had given highest glide score with form I only. So, it is cleared from the result that the paronomycin I exhibits the highest binding affinity against COVID-19. So, these docked complexes of both proteins with paronomycin I had been further utilized for molecular dynamic simulation.

The 2D diagrams from ligand-protein interactions of docked complexes were evaluated for examining the residues involved in binding with paronomycin I (Figure 4B). It has been observed that protease (6y84) shows total 9 hydrogen bonds, 2 salt bridges and 3 carbon-hydrogen bonds with a few van der wall interactions with paronomycin I. As it is clearly depicted from the interaction diagram that Cys-145 makes a strong hydrogen bond with protonated amide group of paronomycin I while the His-41 exhibits van der waals interaction in close proximity. Besides these two catalytic residues, Glu-166 makes 2 hydrogen bonds, 2 salt

bridges and 1 carbon hydrogen bond. Other residues in interaction diagram are as Leu-27, Phe-140, Leu-141, Asn-142, Ser-144, His-163, Met-165.

In the 2D diagram of 6vw1-ligand complex, total 7 hydrogen bonds, 2 salt bridges, 5 carbon hydrogen bonds and a few van der waals interactions have been observed (Figure 4A). Residues involved in different interactions types include Lys-403, Asp-405, Asp-406, Arg-408, Gln-409, Ile-418, Tyr-453, Gln-493, Ser-494, Tyr-495, Gly-496, Phe-497, Tyr-505.

3.5. Docking analysis of Acarbose with target proteins

Acarbose is another common drug that showed strong binding affinity against both targets i.e. 6y84 = -13·139 Kcal / mol and 6vw1= -10·649 Kcal / mol (Table 2). Acarbose made total 13 hydrogen bonds, 1 carbon hydrogen bond and also some van der waals interactions with 6vw1 in docked Complex-3 (Figure 5A). The interacting residues are Ly-403, Asp-406, Gln-409, Tyr-453, Gln-493, Tyr-495, Gly-496, Phe-497, Asn-501, Tyr-505. In case of 6y84, Acarbose forms 10 hydrogen bonds, 1 carbon hydrogen bond, 1 alky bond and other non-covalent interactions in complex 4 (Figure 5B). Residues involved in those interactions are as follow: Thr-26, His-41, Ser-46, Met-49, Leu-141, Asn-142, Ser-144, Cys-145, His-164, Met-165, Glu-166, Pro-168, Arg-188, Gln-189, Thr-190, Gln-192.

3.6. Stability of Complexes by MD analysis

3.6.1. Molecular Mechanics Poisson-Boltzmann Surface Area method (MMPBSA)

MD simulation of complex-1 (6vw1-ligand) and complex-2 (6y84-ligand) along with individual proteins without ligands (6vw1: Protein-1, 6y84: Protein-2) was carried out to record the trajectories for 50 ns. MM/PBSA model was generated using CaFE1.0 VMD plugin. The net binding energy for the complex-1 and complex-2 are -18.3624 kcal / mol and -234.0711

respectively that shows both the complexes are stable (Table 3). The stability of the complex-1 is favored by electrostatic (-25.7727 kcal/mol), van der Waals (-18.0870 kcal/mol) and non-polar energies (-22.0747 k cal/ mol). In case of complex-2, the net binding energy is highly contributed by electrostatic energy (-451.4246 kcal / mol) and less by van der Waals (-37.7393 kcal / mol).

3.6.2. RMSD and RMSF calculations

In order to determine time-dependent conformational changes, RMSD analysis was performed in RMSD trajectory tool of VMD. RMSD graphs were generated with respect to 5000 frames (50 ns) using backbone of their initial structures as reference. Average RMSD of complex-1 was found to be 1·413 ± 0·180 Å while average RMSD of the protein-1 was calculated to be 1·245 ± 0·140 Å. It has been observed that maximum RMSD value never exceeded 1.8 Å during simulation which means that complex-1 remained stable for the entire simulation period. For complex-1, RMSD gradually increased till 28 ns with a drift at 30 ns suggesting some structural changes but complex remains stable and converged after 35 ns (Figure 6A). For complex-2, average RMSD was calculated 1·150 ± 0·157 Å, while the average RMSD of the protein-2 was analyzed to be 1·443 ± 0·280 Å. Complex-2 was also found to be stable as maximum RMSD never exceeded 2 Å for the entire simulation period. In case of complex-2 the RMSD value increased till 32 ns and converged afterwards with minor fluctuations (Figure 6B).

Per residue RMSFs were calculated for the last 10ns in timeline plugin of VMD using comparative approach (Figure 7). In case of complex-1, binding pocket region (400-505) was divided into three interacting regions (1) 403-418 residues, (2) 453-455 residues and (3) 493-505 residues. In the first region of complex-1, Pro-412 (0.39/0.27 Å complex-1/protein-1) and Gly-413 (0.38/0.17 Å complex-1/protein-1) showed drift in RMSF values that could be due to two

hydrogen bond formations by Asp-406 and Gln-409 with the ligand in this region. In region 2, Arg-454 and Leu-455 showed higher RMSFs than protein-1 possibly due to contribution of two hydrogen bonds by Tyr-453 and van der waals interaction by Leu-455. Prior to region 3, Pro-492 exhibited very higher fluctuation in complex-1 (0.41 Å) in addition to Ser-494 (0.21 Å) and Thr-500 (0.36 Å) inside the region in comparison to the respective positions in protein-1. All other interacting residues, except above mentioned, had comparable or even lower fluctuations as compared to unliganded protein. Lower RMSF values of these residues could be related to the rigidity of these residue for any motion due to presence of ligand that contributes stability and loss of flexibility (Chen et al. 2018). In case of complex-2, four interacting regions were found, (1) 140-146 residues, (2) 163-168 residues (3), 25-27 residues, and (4) 41-49 residues. In region 1, Cys-145 shows higher fluctuation in complex-2 (0.3 Å) than in protein-2 (0.25 Å). Glu-166 did not show any prominent variation in complex-2 but its neighboring residue Met-165 and Leu-167 had higher residual fluctuations. Region 3 and 4 contributes through van-der-waals interactions with the ligand and showed no major residual fluctuations. All over both the complexes exhibited lower RMSF values referring to less motion in the binding region conferring their stability.

3.6.3. **Hydrogen Bond interactions**

The hydrogen bond interactions of the complexes were calculated to validate affinity of the ligand to inhibit the proteins predicted by the docking simulation studies. For this purpose two strategies were opted. In the first strategy, total number of hydrogen in complexes and proteins were examined for comparative purpose (Figure 8). Based on the result, complex-2 had higher number of hydrogen atoms than protein-1 while complex-1 and protein-1 exhibited almost comparable hydrogen bonds. In the second strategy, number of hydrogen bonds between receptor

and ligand in complexes (acceptor/donor) were calculated and matched for the identity with the hydrogen bond residues predicted by docking analysis (Table 4). It was validated that the residues involved in hydrogen bonding during post simulation analysis of trajectories were same residues contributing in hydrogen bonding during docking analysis.

4. Discussion

In the present study, it has been observed that none of the anti-malarial drugs showed strong binding affinity with active sites of either protease or RBD. Considering novelty of the virus, blind docking was performed with anti-malarial drugs to further elucidate. Again, no significant binding have been observed as evident from the glide score (Table 1, S1-S4). We confirm that no anti-malarial drug show strong binding affinity for the COVID-19 using molecular docking analysis.

Molecular docking analysis of FDA approved drugs showed that Paromomycin could bind both protease and RBD effectively so it was selected for subsequent studies. Previous studies have used single target approach for targeting corona, either using protease or spike protein (RBD) as targets (Ortega et al. 2020; Xia et al. 2020). Here in this study, we target both the catalytic and RBD domains side by side using a single drug i.e. Paromomycin. This dual targeted approach could have many advantages over single target approach. The potential benefits of this strategy are: it may keep the virus from binding the receptor (ACE2) and at the same time halting the replication of the virus by binding to the catalytic domain of protease.

In the catalytic domain, Paromomycin not only interact with His-41 and Cys-145 but also with Glu-166. Besides two key catalytic residues, Glu-166 is also considered to play a central role in maintaining the shape of protease (S1) catalytic pocket rendering it in active form (Zhang

et al. 2020b). Further analysis of the complex-2 using MD validated its stability. It is also evident from the binding energies of the complex-2 that it is highly stable in the presence of the ligand. Further validation of high binding energy was supported by hydrogen bond analysis of MD trajectories. Complex-2 showed 14 hydrogen bonds between ligand and protease that is well supported by the values of free binding energy.

In case of spike protein, complex-1 showed strong binding affinity with the said residues. Some residues such as Asn-439, Asn-501, Gln-493, Gly-485, Phe-486 and Arg-408, Gln-409, Thr-445, Val-417, Leu-461, Asp-467, Ser-469, Leu-491, Asn-492, Asp-493, Tyyr-494, Thr-497, Thr-150, Tyr-504 are also considered important during interaction with receptors (ACE2 and CD26) (Lu et al. 2020; Vankadari and Wilce 2020). So these residues must also take into account for suggesting a drug against RBD. Paromomycin binding site with RBD showed interaction involving many of these residues in our study. Overall, binding energy and number of hydrogen bonds in complex-1 are lower than that of ccomplex-2, but still it shows good stability in the presence of ligand and can be considered well inhibited by it.

In addition to Paromomycin, Acarbose, an anti-diabetic drug, was also found to show strong binding affinity for both target proteins. As this drug is used for diabetic population so we propose that it could be tested at clinical levels on diabetic patients suffering from COVID-19.

Paromomycin, a broad spectrum aminoglycoside antimicrobial that is originally used to treat acute and chronic intestinal infection may also be potentially used to treat COVID-19. We propose that Paromomycin can be tested to reposition its therapeutic target for the treatment of COVID-19.

Declaration of interests

The authors declare that they have no known competing financial interests or personal relationships that could have appeared to influence the work reported in this paper.

Funding. This research did not receive any specific grant from funding agencies in the public, commercial, or not-for-profit sectors.

Competing interests. The authors declare that they have no competing interests.

Ethical approval and consent to participate. Not applicable.

Acknowledgments. The authors acknowledge Schrödinger https://www.schrodinger.com/ for providing free license for Maestro suits 2019-4 on humanitarian basis particularly for this work. We also thank drugbank https://www.drugbank.ca for permitting us to access to the list of FDA approved drugs.

References

Brooks BR, III CLB, Jr ADM, Nilsson L, Petrella RJ, Roux B, et al. CHARMM: The Biomolecular Simulation Program. J Comput Chem. 2009;30(10):1545–614.

Chen L, Xiong J, Bao L, Shi Y. Convalescent plasma as a potential therapy for COVID-19. Lancet Infect Dis [Internet]. 2020a;20(4):398–400. Available from:

http://dx.doi.org/10.1016/S1473-3099(20)30141-9

Chen Y, Chen X, Luo G, Zhang X, He W, Li G, et al. Discovery of Potential Inhibitors of Squalene Synthase from Traditional Chinese Medicine Based on Virtual Screening and In Vitro Evaluation of Lipid-Lowering Effect. molecules. 2018;23(5):1040.

Chen Y, Liu Q, Guo D. Emerging coronaviruses : Genome structure , replication , and pathogenesis. J Med Virol [Internet]. 2020b;92(4):418–23. Available from: https://doi.org/10.1002/jmv.25681

Duan K, Liu B, Li C, Zhang H, Yu T, Qu J, et al. Effectiveness of convalescent plasma therapy in severe COVID-19 patients. Proc Natl Acad Sci. 2020;1–7.

Friesner RA, Murphy RB, Repasky MP, Frye LL, Greenwood JR, Halgren TA, et al. Extra Precision Glide: Docking and Scoring Incorporating a Model of Hydrophobic Enclosure for Protein−Ligand Complexes. J Med Chem. 2006;49(21):6177–96.

Gao J, Tian Z, Yang X. Breakthrough : Chloroquine phosphate has shown apparent efficacy in treatment of COVID-19 associated pneumonia in clinical studies. Biosci Trends. 2020;14(1):72–3.

Ge X, Li J, Yang X, Chmura AA, Zhu G, Epstein JH, et al. Isolation and characterization of a bat SARS-like coronavirus that uses the ACE2 receptor. Nature [Internet]. 2013;503:535–8. Available from: http://dx.doi.org/10.1038/nature12711

Hoffmann M, Kleine-weber H, Schroeder S, Ger NK, Herrler T, Erichsen S, et al. SARS-CoV-2 Cell Entry Depends on ACE2 and TMPRSS2 and Is Blocked by a Clinically Proven Protease Inhibitor. Cell. 2020;1–10.

Hu TY, Frieman M, Wolfram J. Insights from nanomedicine into chloroquine efficacy against COVID-19. Nat Nanotechnol [Internet]. 2020;1–3. Available from: http://dx.doi.org/10.1038/s41565-020-0674-9

Humphrey, William, Andrew Dalke and KS. VMD: visual molecular dynamics. J Mol Graph [Internet]. 1996;14(1):33–8. Available from: http://www.ks.uiuc.edu/Research/vmd/

Jin Z, Du X, Xu Y, Deng Y, Liu M, Zhao Y, et al. Structure of Mpro from COVID-19 virus and discovery of its inhibitors. Nature [Internet]. 2020; Available from: http://dx.doi.org/10.1038/s41586-020-2223-y

Jo S, Cheng X, Islam SM, Huang L. CHARMM-GUI PDB Manipulator for Advanced Modeling and Simulations of Proteins Containing Nonstandard Residues. Adv Protein Chem Struct Biol [Internet]. 2014;96:235–65. Available from: https://doi.org/10.1016/bs.apcsb.2014.06.002

Jo S, Kim T, Iyer VG, Im W. Software News and Updates CHARMM-GUI : A Web-Based Graphical User Interface for CHARMM. J Comput Chem [Internet]. 2008;29(11):1859–65. Available from: http://www.charmm-gui.org/

Kim S, Lee J, Jo S, Iii LB. CHARMM-GUI Ligand Reader and Modeler for CHARMM Force Field Generation of Small Molecules. J Comput Chem [Internet]. 2017;38(21):1879–86. Available from: http://www.charmm-gui.org/?doc=input/pdbreader

Lee J, Cheng X, Swails JM, Yeom MS, Eastman PK, Lemkul JA, et al. CHARMM-GUI Input Generator for NAMD, GROMACS, AMBER, OpenMM, and CHARMM/OpenMM Simulations Using the CHARMM36 Additive Force Field. J Chem Theory Comput.

2016;12(1):405–13.

Li Y, Cong Y, Feng G, Zhong S, Zhang JZH, Sun H, et al. The impact of interior dielectric constant and entropic change on HIV-1 complex binding free energy prediction. Struct Dyn. 2018;5(6):064101.

Liu H, Hou T. CaFE : a tool for binding affinity prediction using end-point free energy methods. Bioinformatics. 2016;32(14):2216–8.

Lu R, Zhao X, Li J, Niu P, Yang B, Wu H, et al. Genomic characterisation and epidemiology of 2019 novel coronavirus : implications for virus origins and receptor binding. Lancet [Internet]. 2020;395(10224):565–74. Available from: http://dx.doi.org/10.1016/S0140-6736(20)30251-8

Ortega JT, Serrano ML, Pujol FH, Rangel. HR. Unrevealing sequence and structural features of novel coronavirus using in silico approaches: The main protease as molecular target. EXCLI J. 2020;19(Savarino 2005):400–9.

Phillips JC, Braun R, Wang WEI, Gumbart J, Tajkhorshid E, Villa E, et al. Scalable Molecular Dynamics with NAMD. J Comput Chem [Internet]. 2005;26(16):1781–802. Available from: http://www.ks.uiuc.edu/Research/namd/

Sastry GM, Adzhigirey M, Sherman W. Protein and ligand preparation : parameters , protocols , and influence on virtual screening enrichments. J Comput Aided Mol Des. 2013;27:221–34.

Vankadari N, Wilce JA. Emerging WuHan (COVID-19) coronavirus : glycan shield and structure prediction of spike glycoprotein and its interaction with human CD26. Emerg Microbes Infect ISSN. 2020;9(1):601–4.

Wan Y, Shang J, Graham R, Baric RS, Li F. Receptor Recognition by the Novel Coronavirus from Wuhan : an Analysis Based on Decade-Long Structural Studies of SARS Coronavirus. J Virol. 2020;94(7):1–9.

Wang M, Cao R, Zhang L, Yang X, Liu J, Xu M, et al. Remdesivir and chloroquine effectively inhibit the recently emerged novel coronavirus (2019-nCoV) in vitro. Cell Res. 2020;30(3):269–71.

Wang W, Kollman PA. Free Energy Calculations on Dimer Stability of the HIV Protease using Molecular Dynamics and a Continuum Solvent Model. J Mol Biol. 2000;303(4):567–82.

WHO. Coronavirus disease 2019 (COVID-19) Situation Report – 83. 2020.

Wu F, Zhao S, Yu B, Chen Y-M, Wang W, Song Z-G, et al. A new coronavirus associated with human respiratory disease in China. Nature. 2020;579(7798):265–9.

Xia S, Liu M, Wang C, Xu W, Lan Q, Feng S, et al. Inhibition of SARS-CoV-2 (previously 2019-nCoV) infection by a highly potent pan-coronavirus fusion inhibitor targeting its spike protein that harbors a high capacity to mediate membrane fusion. Cell Res. 2020;30(4):343–55.

Xintian X, Ping C, Jingfang W, Jiannan F, Hui Z, Xuan L, et al. Evolution of the novel coronavirus from the ongoing Wuhan outbreak and modeling of its spike protein for risk of human transmission. Sci China Life Sci. 2020;63(3):457–60.

Zhang H, Penninger JM, Li Y, Zhong N, Slutsky AS. Angiotensin‐converting enzyme 2 (ACE2) as a SARS‐CoV‐2 receptor : molecular mechanisms and potential therapeutic target. Intensive Care Med [Internet]. 2020a;46:586–590. Available from:

https://doi.org/10.1007/s00134-020-05985-9

Zhang L, Lin D, Sun X, Curth U, Drosten C, Sauerhering L, et al. Crystal structure of SARS-CoV-2 main protease provides a basis for design of improved α -ketoamide inhibitors. Science (80-). 2020b;3405:1–9.

Zhou P, Yang X, Wang X, Hu B, Zhang L, Zhang W, et al. A pneumonia outbreak associated with a new coronavirus of probable bat origin. Nature [Internet]. 2020;579(7798):270–3. Available from: http://dx.doi.org/10.1038/s41586-020-2012-7

Schrödinger Release 2019-4: Protein Preparation Wizard; Epik, Schrödinger, Prime, Schrödinger, LLC, New York, NY, 2020.

Figure 1. Schematic representation of Study.

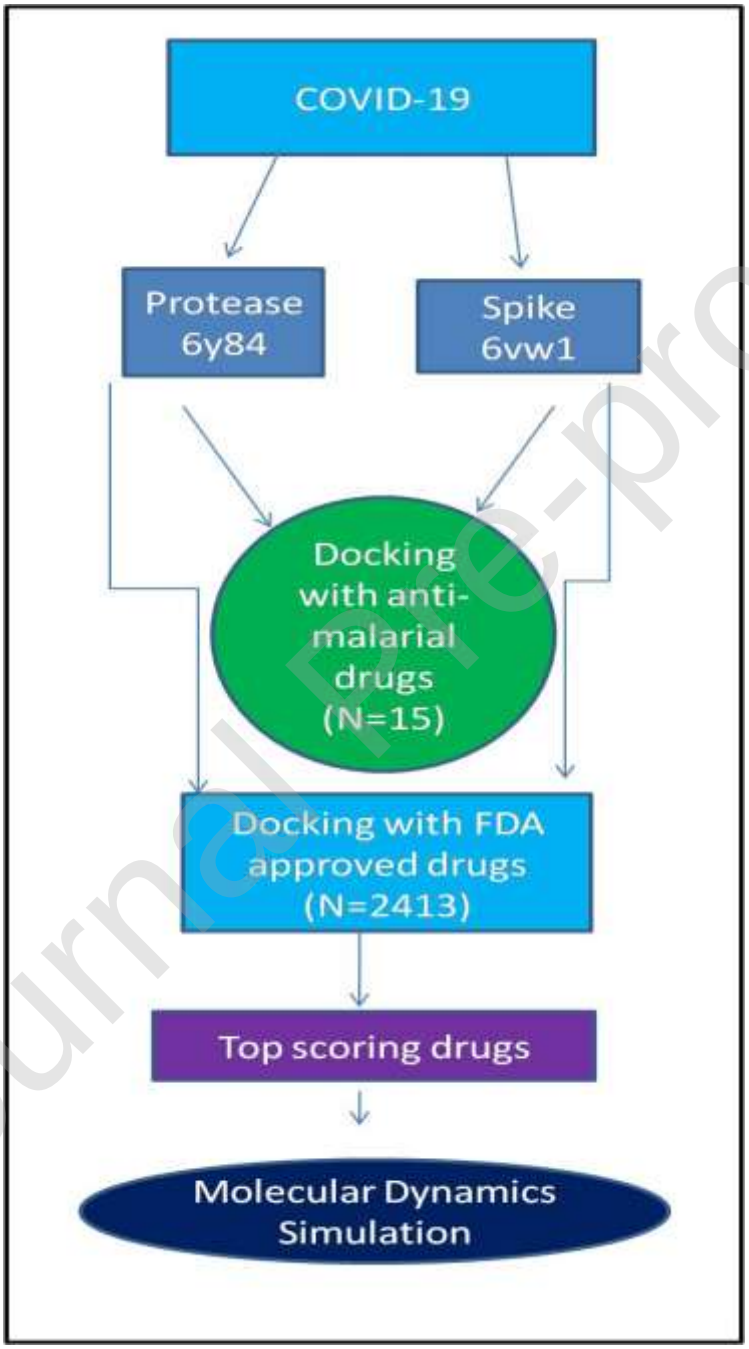

Figure 2. Structural aspects of 6vw1. A: RBD (E chain) of 6VW1 shown in CPK representation while ACE2 (A chain) is shown in Line representation. B: Only RBD (E Chain) shown in Line representation with active residues in CPK representation.

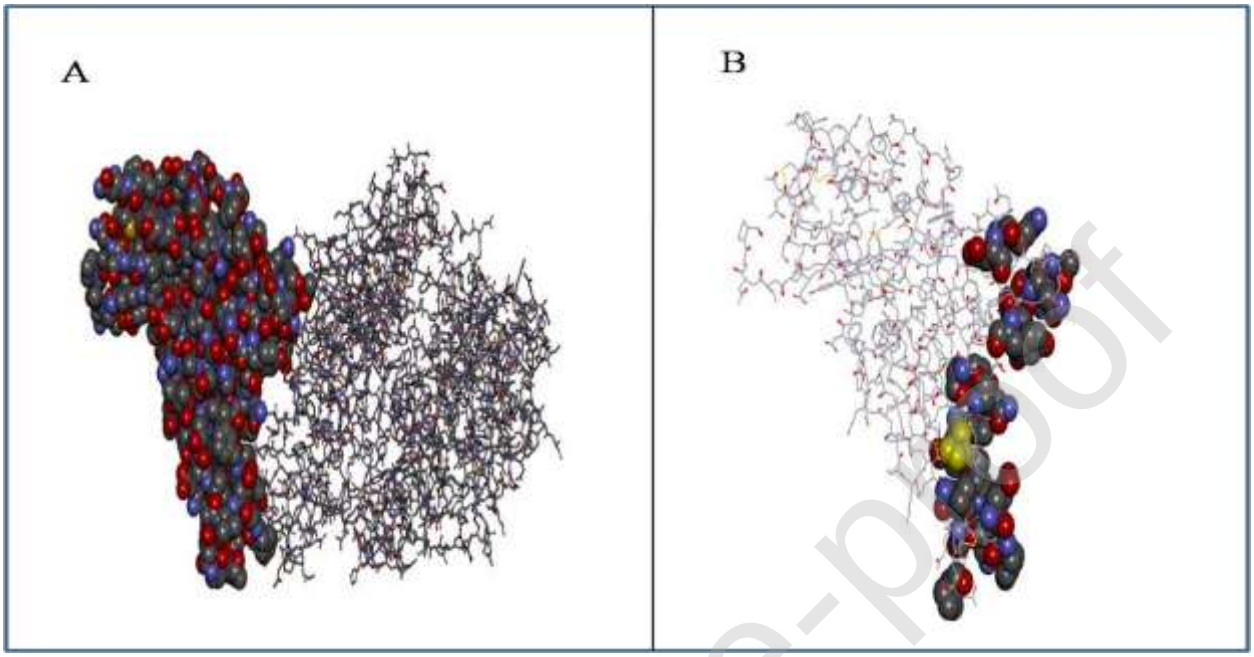

Figure 3. Distribution Plot of docking scores for all the FDA approved drugs dataset used.

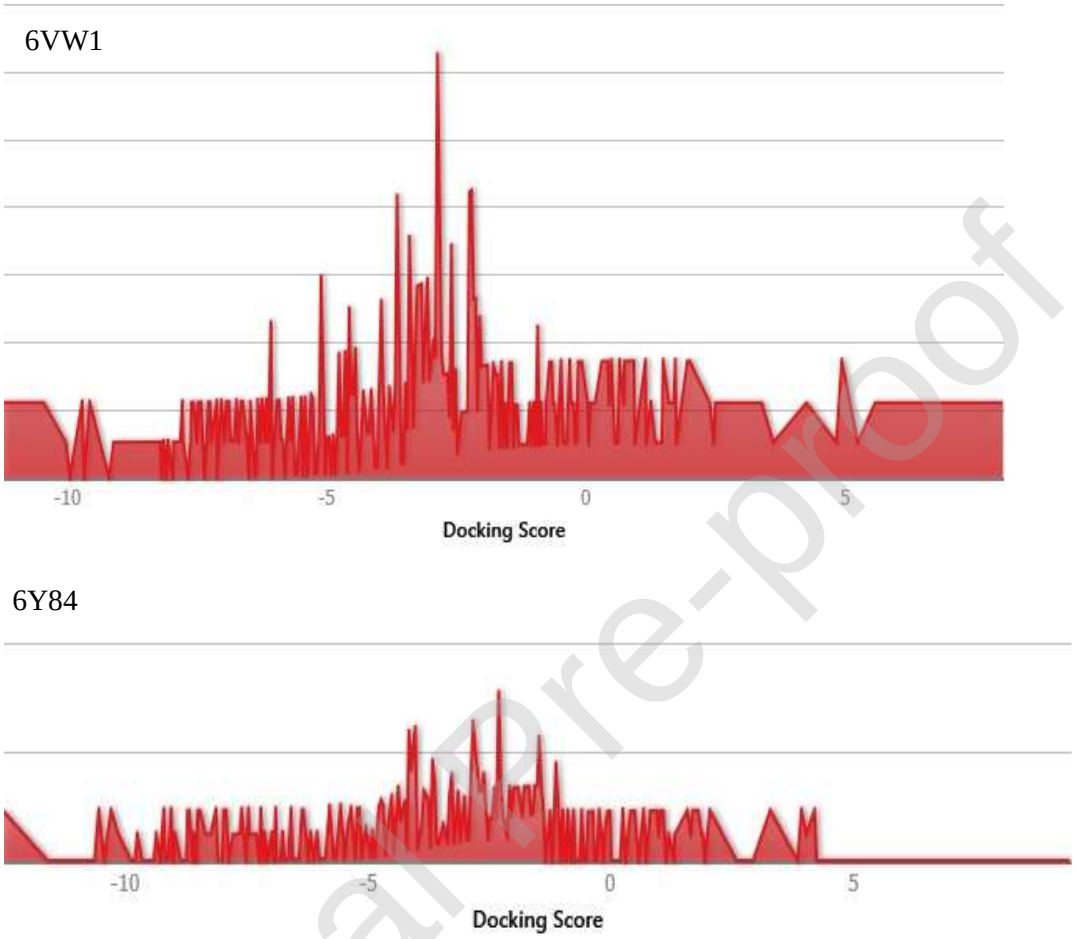

Figure 4. 2D diagram of (A) 6vw1-liagnd (complex-1) and (B) 6y84-ligand (complex-2).

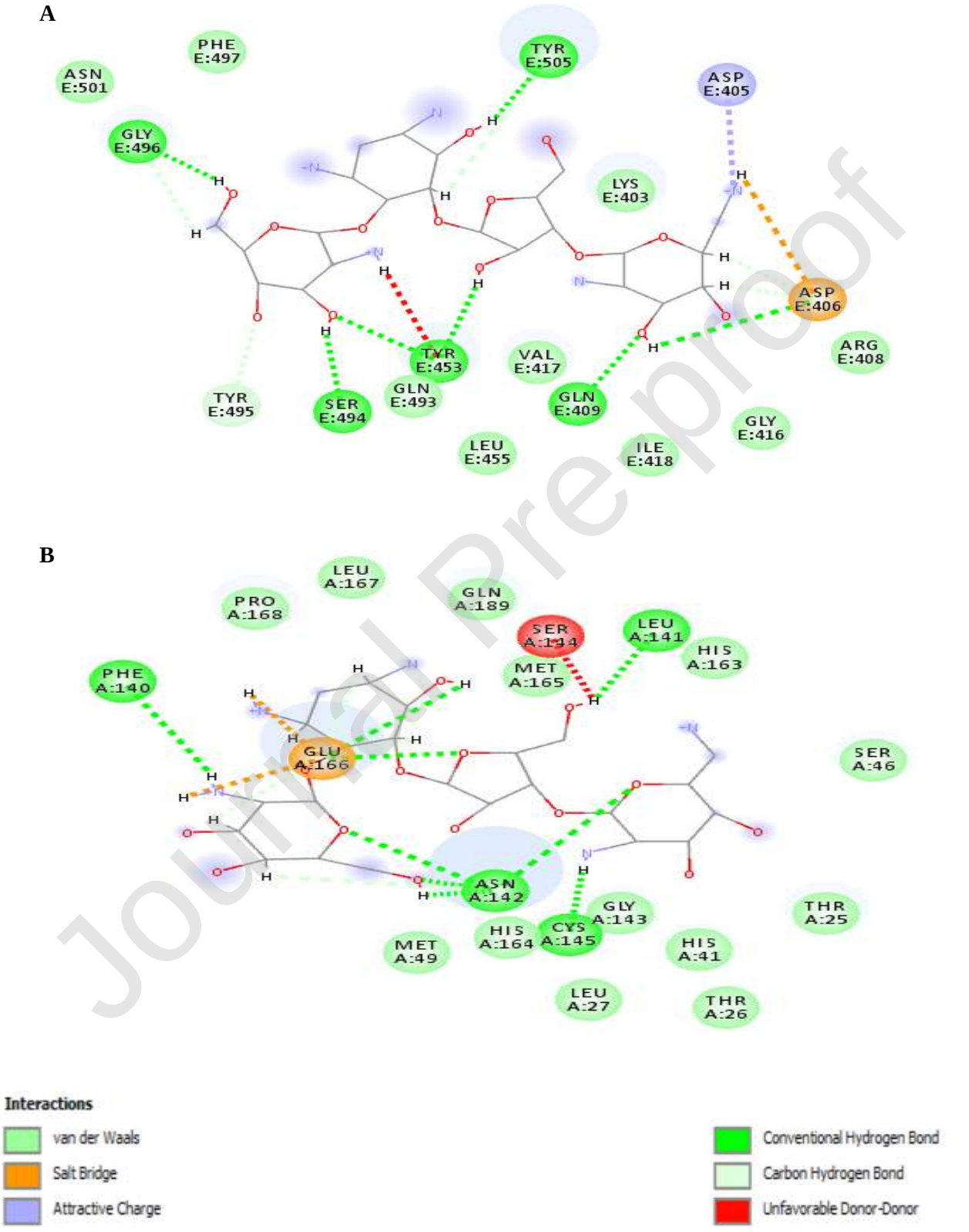

Figure 5: 2D diagram of (A) 6vw1-ligand (Complex-3) and (B) 6y84-ligand (Complex-4).

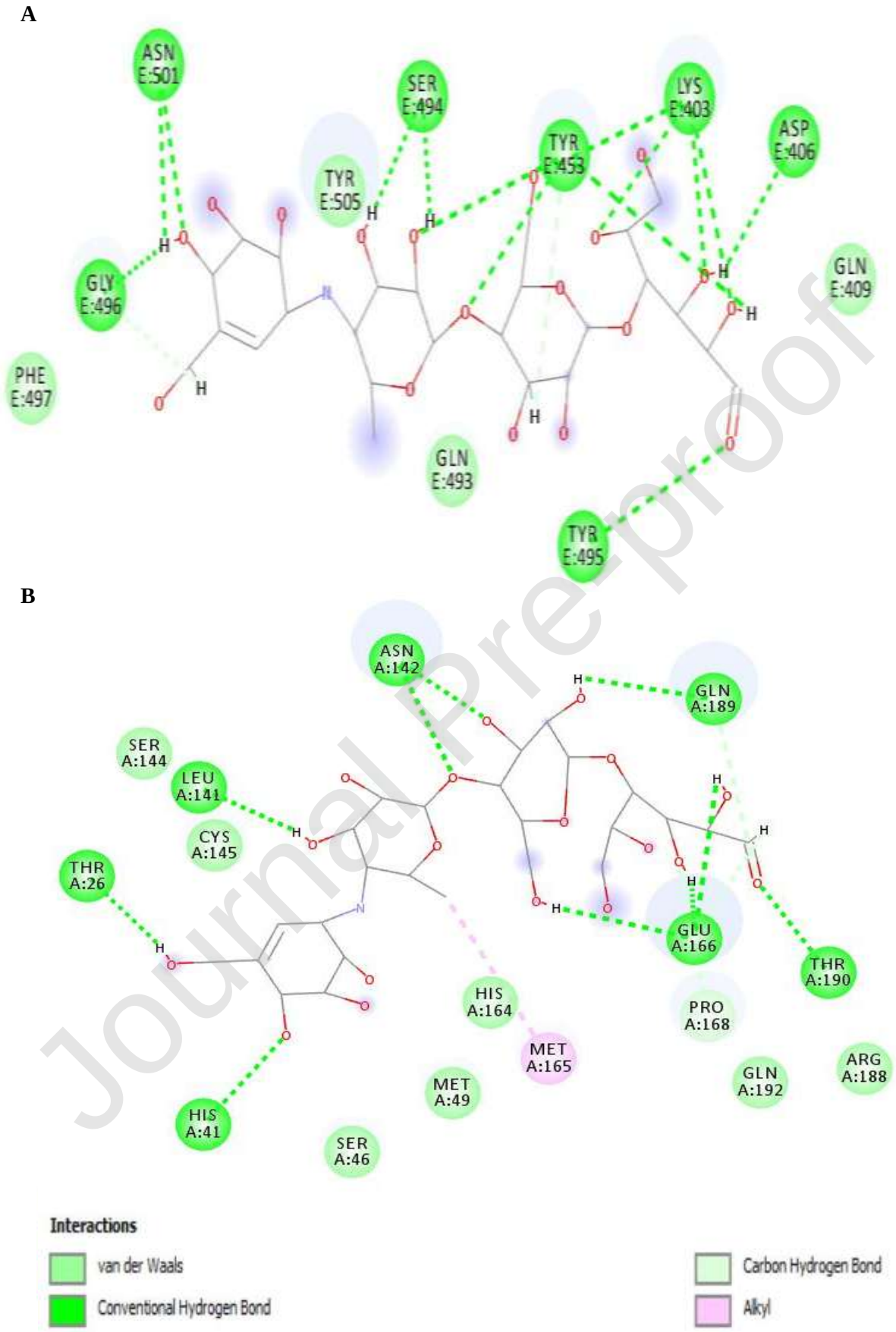

Figure 6: RMSD plot. A: Complex-1 in comparison to Protein-1. B: Complex-2 in comparison to Protein-2.

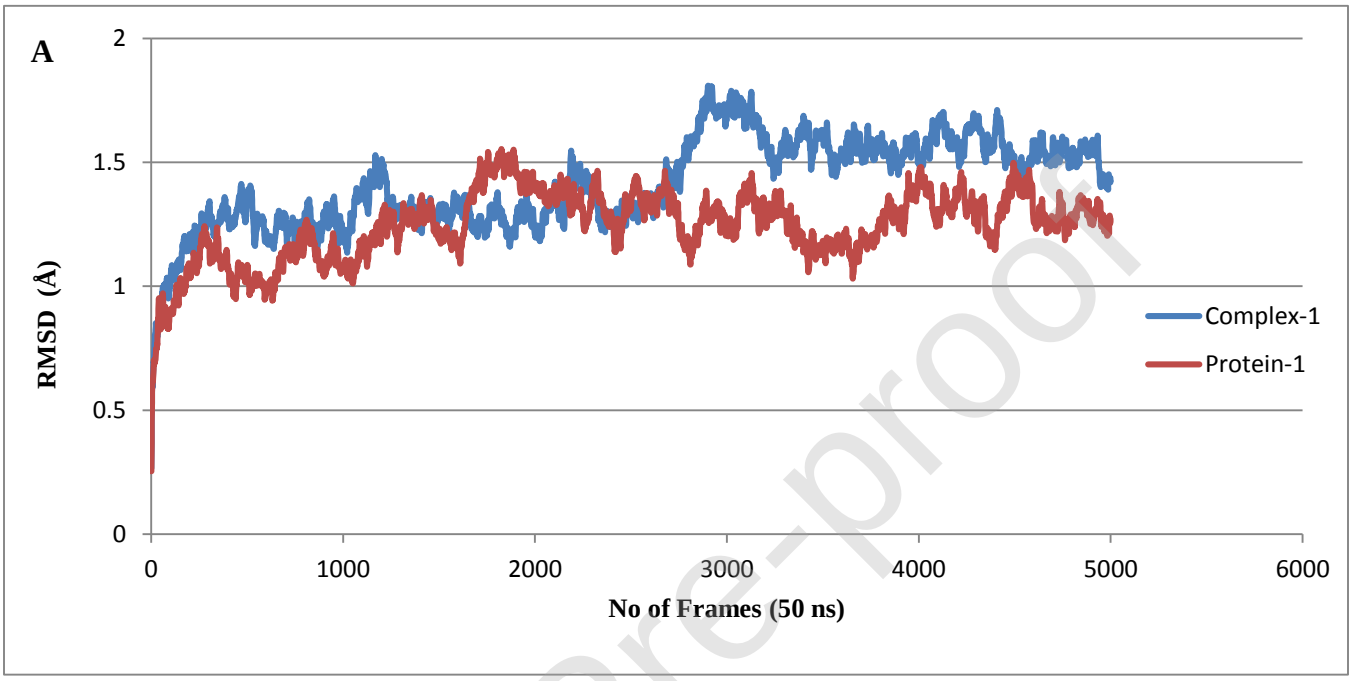

Figure 7. Comparative RMSF plot of (A) complex-1 and protein-1;and (B) complex-2 and protein-2.

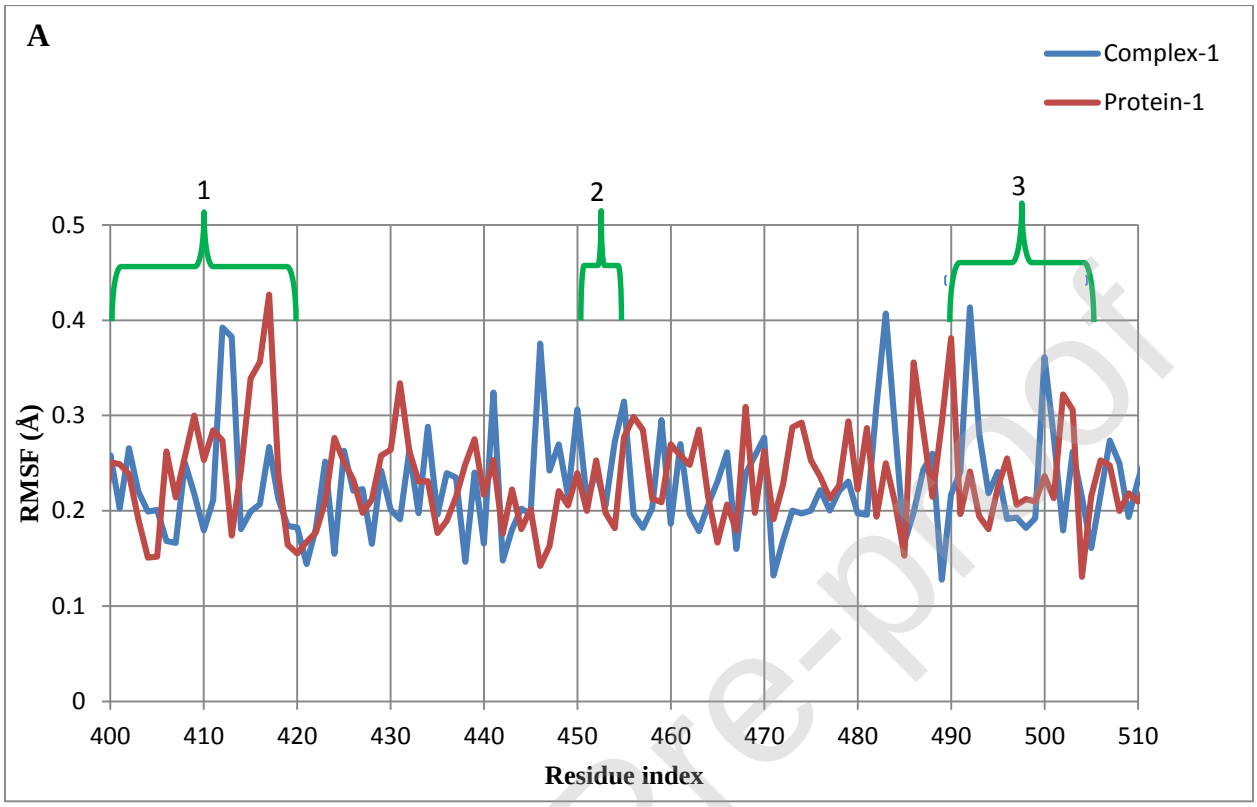

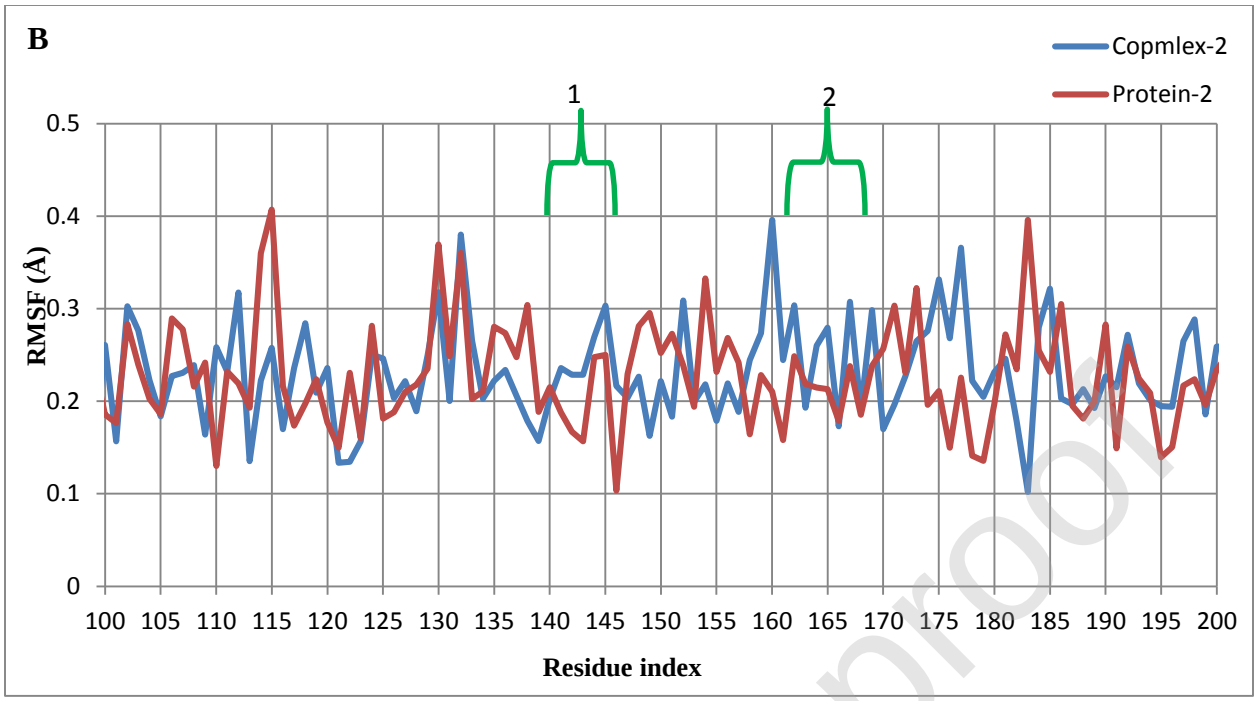

Figure 8. Total hydrogen bonds during the time course of MD simulation.

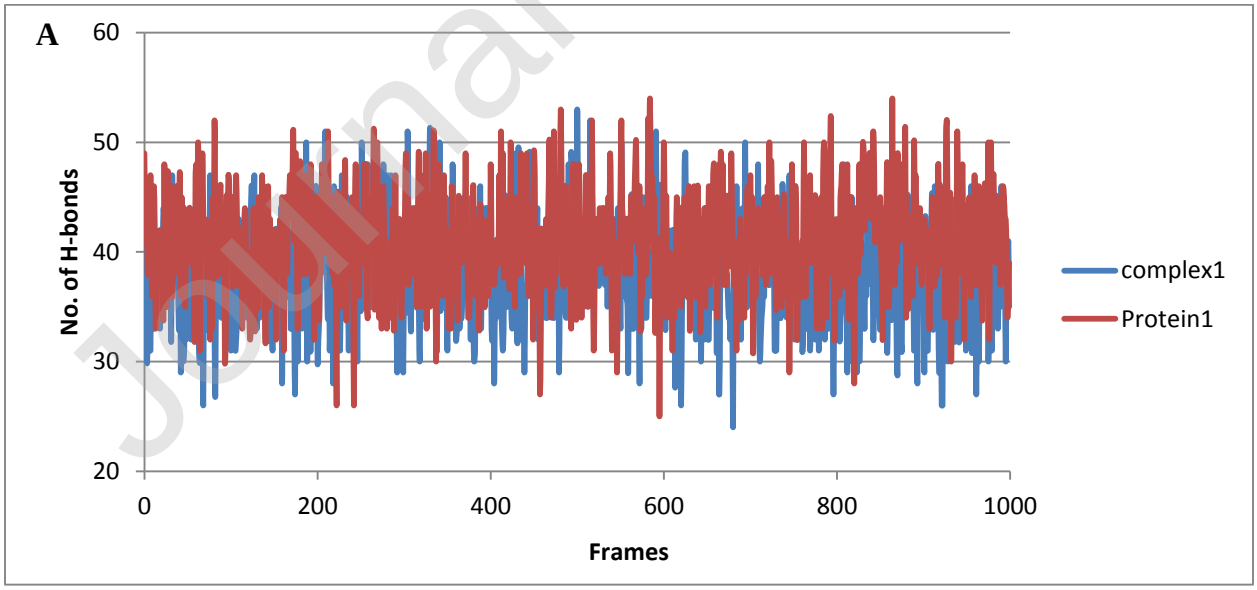

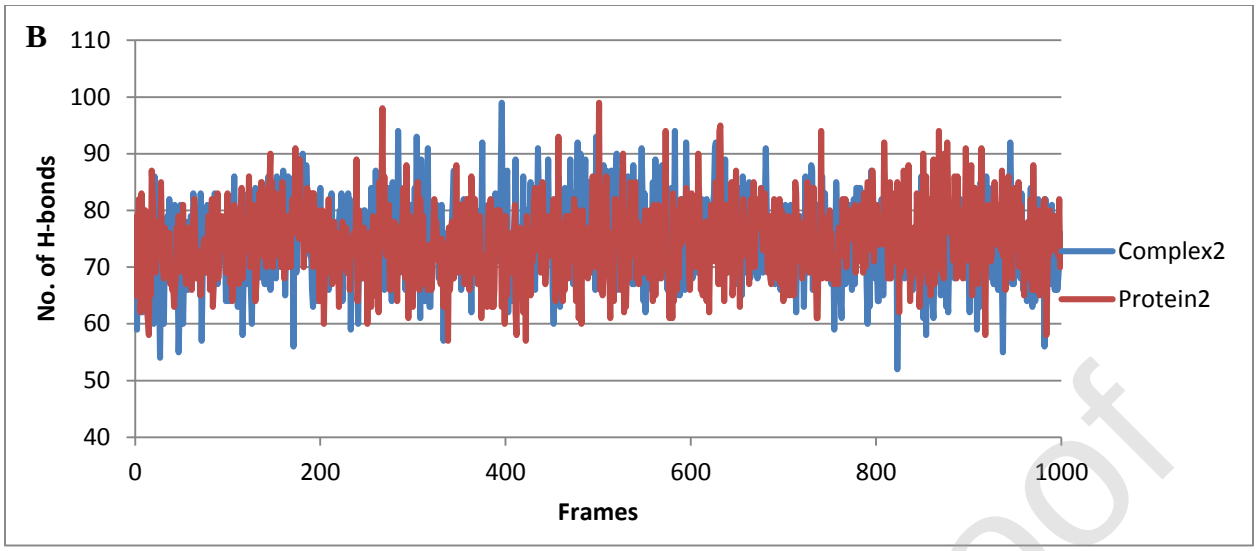

Table 1. Antimalarial drugs against Protease and RBD of COVID-19.

List of antimalarial drugs used			**Glide Score (Grid for specified residues)**		**Glide Score (Global docking)**	
Sr. no.	Name	Pubchem CID	6y84	6vw1	6y84	6vw1
1	Amodiaquin (Flavoquine)	2165	-4·814	-3·211	-5·545	-4·200
2	Chloroquine	2719	-4·111	-2·908	-4·831	-3·828
3	Primaquine	4908	-4·165	-3·111	-5·498	-3·630
4	Pyrimethamine	4993	-3·634	-5·063	-5·403	-3·682
5	Halofantrine	37393	-3·992	-3·656	-4·765	-3·636
6	(-)-Mefloquine	40692	-3·940	-3·014	-4·521	-4·599
7	Artemisinin	68827	-3·992	-2·769	-4·162	-4·786
8	DidesethylChloroquine	122672	-4·968	-3·018	-6·296	-4·050
9	Atovaquone	74989	-3·386	-2·394	-3·727	-3·024
10	Clindamycin	446598	-5·558	-3·466	-5·005	-3·866
11	(S)-Chloroquine	639540	-4·111	-2·908	-4·831	-3·828
12	Quinine	3034034	-4·238	-2·793	-4·491	-3·038
13	Sulfonamides	3085933	-2·545	0·356	-3·871	-3·620
14	Proguanil (Chloroguanide)	6178111	-4·127	-2·328	-1·737	-5·129
15	Doxycycline	54671203	-5·782	-3·749	-6·831	-4·869

Table 2. FDA approved drug showing high binding affinities against Protease and RBD of COVID-19.

6y84				**6vw1**			
Drug name	**Formula**	**Drug bank Id**	**Glide Score**	**Drug name**	**Formula**	**Drug bank Id**	**Glide Score**
Acarbose	C25H43NO18	DB00284	-13·139	Framycetin	C23H46N6O13	DB00452	-11·233
Colistin	C52H98N16O13	DB00803	-12·63	Acarbose	C25H43NO18	DB00284	-10·649
Paromomycin	C23H45N5O14	DB01421	-11·579	Paromomycin	C23H45N5O14	DB01421	-10·01

Iotrolan	C37H48I6N6O18	DB09487	-11·001	Plazomicin	C25H48N6O10	DB12615	-9·935
Indium In-111 pentetreotide	C62H80InN12O19S2	DB11835	-10·795	Omadacycline	C29H40N4O7	DB12455	-9·178
Framycetin	C23H46N6O13	DB00452	-10·713	Mangafodipir	C22H30MnN4O14P2	DB06796	-9·089
Lutetium Lu 177 dotatate	C65H87LuN14O19S2	DB13985	-10·607	Flavin adenine dinucleotide	C27H33N9O15P2	DB03147	-8·986
Rutin	C27H30O16	DB01698	-9·853	Ribostamycin	C17H34N4O10	DB03615	-8·781

Table 3. MMPBSA model for complex1 and complex2.

MMPBSA model	**Complex1**	**Complex2**
Elec	-25.7727 ± 14.0375	-451.4246 ± 16.3534
Vdw	-18.0870 ± 2.9519	-37.7393 ± 3.4501
PB	29.4849 ± 6.9718	261.2760 ± 8.1962
SA	-3.9877 ± 0.1210	-6.1831 ± 0.1261
Gas	-43.8596 ± 13.5039	-489.1639 ± 16.2019
Sol	25.4972 ± 6.9007	255.0928 ± 8.1390
Pol	3.7122 ± 8.5699	-190.1487 ± 9.4145
Npol	-22.0747 ± 2.9860	-43.9224 ± 3.4572
ΔG_{bind}	-18.3624 ± 7.5918	-234.0711 ± 8.9385

.

Table 4. Total hydrogen bonds between receptor and ligand determined from MD trajectories.

Complex-1		**Complex-2**	
Donor	Acceptor	Donor	Acceptor
UNK900-Side	Asp406-Side	UNK1-Side	Glu166-Main
Tyr505-Side	UNK900-Side	UNK1-Side	GluU166-Side
UNK900-Side	Gln09-Side	Glu166-Main	UNK1-Side
Tyr453-Side	UNK900-Side	Asn142-Side	UNK1-Side

Gln409-Side	UNK900-Side	UNK1-Side	Asn142-Side
		UNK1-Side	Phe140-Main
		UNK1-Side	Gln189-Side
		UNK1-Side	Cys145-Side
		UNK1-Side	Ser46-Side
		UNK1-Side	Leu141-Main
		Gln189-Side	UNK1-Side
		UNK1-Side	Ser144-Side
		UNK1-Side	Thr25-Side
		UNK1-Side	His41-Side